Nanoparticles induce dermal and intestinal innate immune system responses in zebrafish embryos

Brun, N.R.; Koch, B.E.V.; Varela, M.; Peijnenburg, W.J.G.M.; Spaink, H.P.; Vijver, M.G.

Article details

Brun N.R., Koch B.E.V., Varela M., Peijnenburg W.J.G.M., Spaink H.,P. & Vijver M.G. (2018), Nanoparticles induce dermal and intestinal innate immune system responses in zebrafish embryos, Environmental Science: Nano 5(4): 904-916.
Doi: 10.1039/C8EN00002F

Environmental Science Nano

PAPER

View Article Online
View Journal

Cite this: DOI: 10.1039/c8en00002f

Nanoparticles induce dermal and intestinal innate immune system responses in zebrafish embryos†

Nadja R. Brun, *[ab] Bjørn E. V. Koch,[c] Mónica Varela, [c] Willie J. G. M. Peijnenburg,[ad] Herman P. Spaink[c] and Martina G. Vijver[a]

Major molecular mechanisms that underpin the toxicity of nanoparticles (NPs) are the formation of reactive oxygen species and the induction of inflammation. The latter is frequently observed *in vitro* and in mammalian organisms, yet in aquatic organisms, such NP-induced inflammatory responses remain largely unexplored. Zebrafish offer a wide range of molecular tools to investigate immune responses in an aquatic organism, and were therefore used here to describe how copper (Cu) NPs (25 nm; 1 mg L^{-1}) and soluble Cu as well as polystyrene (PS) NPs (25 nm; 10 mg L^{1-}) induce innate immune responses, focussing on the skin cells and the intestine as likely organs of interaction. mRNA expression of the immune responsive genes *interleukin 1 beta* (*il1β*) and *immunoresponsive gene 1-like* (*irg1l*) of CuNP exposed embryos was observed to be weaker in the intestinal tissue compared to the rest of the body, indicating a strong outer epithelium response. Specifically, NPs were observed to accumulate in the cavities of lateral neuromasts in the skin, which coincided with an increased local expression of *il1β*. Exposure to CuNPs triggered the strongest transcriptional changes in pro-inflammatory-related genes and was also observed to increase migration of neutrophils in the tail, indicating a NP-specific inflammatory response. This is the first *in vivo* evidence for waterborne NP exposure triggering alterations of immune system regulating genes in the skin and intestine of zebrafish embryos. The observed molecular responses have the potential to be linked to adverse effects at higher levels of biological organization and hence might be used for screening purposes in nanotoxicology or as building blocks for adverse outcome pathways.

Received 1st January 2018,
Accepted 4th March 2018

DOI: 10.1039/c8en00002f

rsc.li/es-nano

Environmental significance

Increasing our understanding of how nanoparticles affect organisms is essential to predict and mitigate environmental threats, yet to date little is known about their potential to affect immune systems in aquatic organisms. In this work, primary sites of metallic and plastic nanoparticle accumulation and their potential to induce an inflammatory response are explored in zebrafish embryo. This study provides initial evidence that nanoparticles accumulate on the external and internal epithelium, and can elicit transcription of pro-inflammatory cytokines in zebrafish embryos. This can potentially be used as a building block in developing adverse outcome pathways for nanoparticles in ecological risk assessment.

Introduction

Nanoparticles (NPs) pose a potential risk to ecosystems and the organisms living therein due to widespread use in medical and consumer products, and subsequent gradual release into the environment. An increasing number of studies are therefore aimed at understanding of uptake routes, bioaccumulation potential, and mode of actions of NPs. However, formulating a general framework for risk assessments is currently hampered by the plethora of variables affecting NP bioavailability and toxicity, including different core compositions, shapes, sizes and surface modifications.[1] An emerging approach in risk assessment is therefore, to unravel shared molecular responses caused by exposure as this can be linked to adverse effects at higher levels of biological organization, a concept known as adverse outcome pathways (AOPs).[2]

Two major molecular pathways are commonly affected by exposure to particles in the nanometer range: oxidative stress and inflammation. Generation of reactive oxygen species (ROS) fuelled by NPs or metal ions dissolved from NPs is a key mechanism of NP toxicity that is frequently observed and

[a] *Institute of Environmental Sciences (CML), Leiden University, Leiden, The Netherlands. E-mail: n.r.brun@cml.leidenuniv.nl*
[b] *Department of Biology, Woods Hole Oceanographic Institution, Woods Hole, MA, USA*
[c] *Institute of Biology, Leiden University, Leiden, The Netherlands*
[d] *National Institute of Public Health and the Environment (RIVM), Center for Safety of Substances and Products, Bilthoven, The Netherlands*

† Electronic supplementary information (ESI) available. See DOI: 10.1039/c8en00002f

is currently the best-understood mechanism,[3–5] in which the formation of highly reactive oxygen radicals can disturb mitochondrial function ultimately leading to apoptosis.[6,7] However, metals and NPs are also recognized as a potent inducer of immune and inflammatory responses.[8] Epithelial and mucosal linings are major components of the innate immune system and are the site where NPs may be recognized as pathogens by the Toll-like receptors, triggering innate immune responses in the organism and leading to induction of pro-inflammatory genes such as interleukins, cytokines, and chemokines.[9] The organism's response culminates in recruiting phagocytic cells (neutrophils and macrophages) to the site of infection or injury. This suggests that NP-induced inflammation might also serve as a sensitive molecular response, and hence it is key to identify primary sites of induction and relative sensitivity.

In aquatic organisms, it is widely accepted that the NPs first target the outer skin and the intestine,[10] which correlates with the primary sites where the innate immune system can be activated. On the external epithelial membranes of fish, NPs can interfere with the lateral line system, inducing oxidative stress or apoptotic cell death in neuromasts, ultimately leading to a reduction of functional neuromasts and attenuated orientation within a current.[11–13] Although lateral line neuromasts are used for screening purposes to identify immunomodulatory compounds, NPs have not yet been assessed for this activity. In intestines of juvenile fish, an immune response after NP exposure was detected by increased mRNA levels of pro-inflammatory related genes after copper (Cu) NPs exposure.[14] Moreover, the effect was more pronounced for the NP than for the soluble copper exposure. In zebrafish embryos, despite being a widely used organism to screen for NP toxicity or investigate immune responses, target sites of NPs have not yet been explored for such responses. Whole embryo assessment revealed that gold NPs (1.5 nm) alter genes involved in inflammatory pathways after waterborne exposure of dechorionated embryos[15] and injected silica NPs (62 nm) lead to neutrophil-mediated cardiac inflammation.[16] Innate immune responses in early life stages of fish triggered by NPs is thus conceivable, however, the assessment and localization of inflammation as a molecular key event after waterborne exposure of NPs remains largely unexplored.

Zebrafish embryos are due to their transparency a suitable living system to study the dermal and intestinal epithelium as potential sites of action of NPs. More importantly, the zebrafish embryo is a widely used model organism that is well established in immunology and allows for the tracking of fluorescently labeled compounds as well as several key immune responsive genes and cells in different organs.[17] Our aim was to use this aquatic model organism to investigate the two putative sites of NP accumulation, the skin and the intestine, and to compare their potential to elicit an inflammatory response. To disentangle the NP contribution, an inert polystyrene NP (PSNP) and a metallic NP (CuNP), as well as the dissolved metal fraction released from the metal NP, were assessed. While Cu is a metal well-recognized for its potential to elicit an inflammatory response, the toxic mechanism of PSNP remains largely unexplored. An environmentally relevant concentration of fulvic acid was added to stabilize metal particle aggregation, complex toxic Cu^{2+}, and mimic environmentally relevant conditions. The dosage of NPs was based on no observed adverse effects for malformation. Immune responses were subsequently assessed with qPCR and *in situ* hybridization targeting genes from the innate immune responses in whole body, intestine, and body without intestine samples and with transgenic zebrafish lines expressing green fluorescent proteins (GFP) under interleukin 1 beta (*il1β*), tumor necrosis factor alpha (*tnfα*), neutrophil-specific (myeloperoxidase, *mpx*) and macrophage-specific (*mpeg*) promoter.

Materials and methods

Materials

CuNPs (chemical formula: Cu, with a specific surface area of 30–50 $m^2\ g^{-1}$, a purity of 95.5% and a density of 8.92 $g\ cm^{-3}$) with a nominal size of 25 nm were purchased as dry powder from IoLiTec, Inc. (Germany) and copper(II) nitrate ($Cu(NO_3)_2$) from Sigma-Aldrich (The Netherlands) was used as dissolved metal control. Fluorescent polystyrene particles (PSNP; 25 nm, ThermoFisher Scientific, U.S.) were used as an inert NP and to track target organs of particles. The Suwannee River humic acid (SRHA) standard containing 15% fulvic acid and 85% humic acid (International Humic Substances Society, Atlanta, Georgia) was used as a surrogate for organic matter.

SRHA, Cu, and polystyrene nanoparticle characterization

A stock solution of 1000 mg L^{-1} SRHA in egg water (60 mg L^{-1} InstantOcean Sea Salt, Sera Marin) was prepared according to Wang *et al.* (2015).[18] In pre-experiments, the nominal concentration of 30 mg L^{-1} SRHA was determined to decrease particle aggregation (Fig. S1a and b in ESI†) and not to influence normal embryo development (data not shown). The total amount of organic carbon (TOC) in exposure media was analyzed by TOC analysis (Thermo Hiper; ThermoFisher Scientific, U.S.).

Prior to use, both nanoparticles were characterized by size, shape, surface charge, and aggregation. Transmission electron microscopy (TEM; JEOL 1010, JEOL Ltd., Japan) was used to characterize the size and shape of the NPs after 1 hour of incubation in egg water. Size distribution and zeta potential of all exposure samples were measured directly after preparation (0 h) and after 24 h incubation by dynamic light scattering (DLS; Zetasizer, Malvern Instruments, UK). Three independent measurements were performed, each consisting of three repeated measurements. Dissolved Cu concentration from CuNP exposure suspensions was measured over time (0 h, 24 h, and 48 h) using flame atomic absorption spectroscopy (AAS; Perkin Elmer 1100B, The Netherlands) by collecting samples from the suspension and the supernatant (after centrifugation for 20 min at 14 680 rpm at 4 °C) and acidifying it in 10% HNO_3 overnight at room temperature.

Centrifugation at this speed was previously shown to efficiently remove CuNPs from suspension.[19] The measurements were carried out in triplicate. The percentage of dissolution of the CuNPs was then calculated as the percentage of the total copper concentrations. Furthermore, the amount of dissolved Cu in mg L^{-1} was used to derive the corresponding copper nitrate concentration. In order to achieve a copper nitrate stock solution of a known measured concentration, a stock solution of 1 mg mL^{-1} copper nitrate in Milli-Q was prepared. Thereof, serial dilutions ranging from 0.4 to 5 mg L^{-1} were prepared and measured by AAS to calculate a linear standard curve of nominal *versus* measured copper nitrate concentration. The equation derived from linear regression analysis allowed the use of a copper nitrate concentration corresponding to the measured dissolved copper from CuNP.

Modelling of metal speciation

Visual MINTEQ (ver 3.1)[20] was used to model the speciation of 0.59 mg L^{-1} free copper (released from 1 mg L^{-1} CuNP or added as $Cu(NO_3)_2$) in egg water at pH 7.0. The NICA–Donnan model with a specification of 15% solid fulvic acid and 85% humic acid at a concentration of 12.9 mg L^{-1} (according to mean measured concentrations) was applied to calculate the binding of metals by SRHA.

Embryo exposure

Zebrafish were handled in compliance with animal welfare regulations and maintained according to standard protocols (http://ZFIN.org). The culture was approved by the local animal welfare committee (DEC) of the University of Leiden and all protocols adhered to the international guidelines specified by EU Animal Protection Directive 2010/63/EU. Zebrafish eggs were obtained from mixed egg clutches from wildtype ABxTL strain, *Tg*(*mpx:eGFP*),[21] *Tg*(*mpeg1*:*eGFP*),[22] *Tg*(*il1b*:*eGFP-F*),[23] and *Tg*(*tnfa:eGFP-F*)[24] strain. Fertilized eggs were distributed in 6-well plates (20 embryos per well) with 6 ml of exposure solution: control (egg water), control supplemented with SRHA, 0.1 mg L^{-1} CuNP and corresponding copper nitrate concentration, 1 mg L^{-1} CuNP and corresponding copper nitrate concentration, and 10 mg L^{-1} PSNP with 5 replicates in each group. The concentration of NPs was based on no observed adverse effects for malformation derived from pilot studies. The CuNP at a final concentration of 0.1 and 1 mg L^{-1} were dispersed in egg water supplemented with SRHA and the PSNP were dispersed in egg water only. All exposure media were sonicated in an ultrasonic water bath (USC200T, VWR, Amsterdam, The Netherlands) for 5 min prior to exposure.

For the copper uptake experiment and assessment of morphological endpoints (hatching success, developmental anomalies, size, and mortality), ABxTL embryos were exposed in 6-well plates (10 embryos per well, 1 wells per exposure group) from 0 to 120 hpf. Hatching success, developmental anomalies, and mortality was assessed from five independent egg clutches. Exposure medium and egg water were replaced daily and embryos were screened for morphological endpoints using a Leica stereomicroscope (M165 C, Switzerland). At 72 hpf 10 ABxTL embryos per exposure group were sampled for quantification of copper concentrations. At the end of exposure at 120 hpf, 10 hatched ABxTL embryos were imaged for size measurement using the stereomicroscope equipped with a camera (DFC 420) and 5 embryos thereof sampled for copper concentration measurement. The larval size was determined using ImageJ.[25]

For RNA extraction and *in situ* hybridization, hatched embryos were exposed from 72 to 120 hpf in 6-well plates with one exposure medium replacement. At the end of exposure at 120 hpf, 15 embryos per replicate were snap frozen in liquid nitrogen and sampled for RNA extraction. For live imaging of immune responses, a short-term exposure of 24 h and a lower CuNP (0.1 mg L^{-1}) concentration was chosen in addition to the exposure above. A shorter exposure time enables the detection of early inflammatory responses and a lower CuNP concentration of 0.1 mg L^{-1} was chosen, as 1 mg L^{-1} copper could slow down development.

Extraction of the intestine

For organ-specific expression analysis using qPCR, the intestine of 120 hpf embryos was extracted from anesthetized embryos by fixing the anterior part with insect needles and pulling on the jaw using forceps. The tissues were directly placed into Trizol for subsequent RNA extraction. Intestines or bodies without intestine of 10 embryos per group were pooled to one replicate. Three replicates per group (control and 1 mg L^{-1} CuNP) were prepared. Genes of interest with local expression in intestinal tissue were *il1β*, *irg1l*, and *tnfα*.

Quantification of copper concentration in zebrafish embryos

For total Cu quantification in zebrafish embryos, 5 embryos per replicate (n = 3) were collected at 72 hpf and 120 hpf and dechorionated if not hatched. Only viable embryos with no morphological malformations were chosen. Embryos were washed three times with Milli-Q water supplemented with 1 mM EDTA. Once rinsed, embryos were transferred into Eppendorf tubes and excess liquid was removed. Samples were digested in 300 μL *aqua regia* (HNO_3 : HCl; 1 : 3) overnight and subsequently heated to 70 °C to evaporate all liquid. The residue was dissolved in 0,1 n HNO_3 in superdemineralized water and measured by Graphite Furnace Atomic Absorption Spectrometry (GF-AAS; Perkin Elmer, The Netherlands).

RNA isolation, cDNA synthesis, and expression analyses

Total RNA (1 μg) was extracted using trizol (invitrogen) according to manufacturer's protocol, purified on RNeasy MinElute Cleanup columns (Qiagen, The Netherlands) and quantified using a NanoDrop ND-1000 spectrophotometer (Nanodrop Technologies Inc., U.S.). The first strand cDNA was synthesized thereof using the Omniscript™ reverse transcriptase kit (Qiagen, The Netherlands), Oligo-dT primers

(Qiagen), and RNase inhibitor (Promega). cDNAs were then diluted 5 times and reverse transcription-quantitative polymerase chain reaction (RT-qPCR) was conducted with gene-specific primer pairs (Table S1, ESI†) mixed with SYBR Green (iQ supermix, Qiagen, The Netherlands). The samples were denatured for 5 min at 95 °C and then amplified using 40 cycles of 15 s at 95 °C and 45 s at 58 °C or 60 °C (depending on transcript target), respectively, followed by quantitation using a melting curve analysis post run. Amplification and quantification were done with the CFX96 Biorad system and was run with five biological replicates (or three for intestine and body without intestine samples) and two technical duplicates. Fold induction was calculated by normalizing C_T values of the target gene to the C_T value of the housekeeping gene *β-actin* (=ΔC_T) and then normalized to the untreated control (ΔC_T untreated − ΔC_T treated).

In situ hybridization

Wild-type zebrafish embryos (ABxTL strain) were raised in 0.003% 1-phenyl-2-thiourea (PTU; Sigma-Aldrich, The Netherlands) no later than 24 hpf to prevent pigmentation. Hatched embryos were exposed to 10 mg L^{-1} PSNP, 1 mg L^{-1} CuNP and corresponding copper nitrate concentration from 72 to 120 hpf with one medium exchange after 24 h. Embryos were anesthetized with 200 μg mL^{-1} 3-amino-benzoic acid (tricaine; Sigma-Aldrich) on ice and fixed in 4% paraformaldehyde. Whole-mount *in situ* hybridization was performed using a standard protocol.[26] *Irg1l* was tested by two non-overlapping digoxigenin-labeled anti-sense RNA probes produced by PCR amplification and *in vitro* transcription, using the approach previously described.[27] Primer sequences (5′–3′): probe #1 F: CACATGTATGCTTCTGACGACATCAG, probe #1 R: AAGCCC GCTTGGTTTGCTGTTGCTG, probe #2 F: GGGCATTGAAATAC AAGGCCGACTG, probe #2 R: AGATTGTGTTGCAGCATTAGC CATTGG.

Intravenous microinjection

Wild-type zebrafish embryos were treated with PTU from 24 hpf onwards. Embryos were manually dechorionated at 24 hpf and after anesthetizing the embryos, injection was performed at 30 hpf in the blood island with 1 nl of MilliQ (control), 0.5 mg L^{-1} CuNP in MilliQ, or 1 mg L^{-1} PSNP in MilliQ using a Femtojet injector (Eppendorf). All injection solutions contained 1% phenol red and were sonicated before injection. 24 h later, whole body and tail imaging were performed and 15 embryos per replicate snap-frozen for subsequent RNA extraction and qPCR.

Live imaging of immune responses and NP target organs

Distribution of neutrophils and macrophages were visualized using the transgenic zebrafish reporter lines for neutrophils *Tg*(*mpx*:*eGFP*) and macrophages *Tg*(*mpeg1*:*eGFP*) after exposure to 0.1 mg L^{-1} CuNP and 10 mg L^{-1} PSNP from 96–120 hpf. The activation of *il1β* was visualized using the *Tg*(*il1b*:*eGFP-F*) line. Embryos used for stereo fluorescence imaging were kept in egg water containing 0.0003% PTU to prevent pigmentation. Embryos were anesthetized in tricaine for imaging with a Leica stereo fluorescence microscope (M205 FA) equipped with a digital camera (DFC 345 FX). Each image contains 3 channels: bright field, fluorescent green (GFPgreen), and fluorescent red (DRSred). In order to visualize the expression of *il1β* and *tnfα* in the neuromasts and skin cells, *Tg*(*il1b*:*eGFP-F*) and *Tg*(*tnfa*:*eGFP-F*) were exposed as described above but without PTU and then fixed in 4% PFA overnight before being transferred in TBST and subsequent imaging under a Leica SPE confocal using 40× water objective.

Statistical analyses

The data were graphically illustrated with GraphPad Prism 6 (GraphPad Software, U.S.). Variance homogeneity of the data was assessed with Bartlett's test. Fold changes were log2 transformed. Significant differences between treatments were assessed by one-way ANOVA followed by a Bonferroni multiple comparison test ($p \leq 0.05$) to compare treatment means with respective controls. All measurements (TEM, DLS, TOC, AAS) were conducted in triplicates ($n = 3$) except for morphological endpoints including hatching success, developmental anomalies, and mortality (5 independent experiments with 10 embryos each; $n = 5$), size measurement ($n = 10$), qPCR ($n = 3$–5), imaging of *in situ*, microinjections, and reporter lines ($n = 10$) with one representative picture depicted. Results are expressed as means ± standard deviation of the mean (SD). Differences were considered statistically significant at $p \leq 0.05$.

Results

Nanoparticle characterization

The initial particle size of both nanoparticles, CuNP and PSNP, was confirmed to be approximately 25 nm as visualized using TEM (Fig. 1a). Imaging revealed that both particles had a roughly spherical shape. The TEM images revealed single particles and agglomerates for both particles. It should be noted that the picture in Fig. 1a does not reflect a representative cluster size but the picture with the best contrast. Once dispersed in egg water, CuNP agglomerated immediately to clusters with an average hydrodynamic diameter of 291 ± 30 nm and to even bigger clusters of 375 ± 36 nm after 24 h. PSNP, on the other hand, remained stable over time with an average size in the medium of 19.3 ± 0.6 nm after 0 h or 18.8 ± 0.9 nm after 24 h, respectively (Fig. 1b). The zeta potential of both particles remained between −20 and −30 mV over time (Fig. 1c), indicating a continuous negative surface charge and thus repulsion forces keeping the particles in a rather stable suspension. Nevertheless, the CuNP clustered to agglomerates of various sizes.

The major impact of SRHA on CuNP suspension characteristics is the complexation of the free copper ions. The total concentration of Cu^{2+} is reduced from 49.4% in pure egg water to 9.2% in egg water with SRHA as calculated by Visual

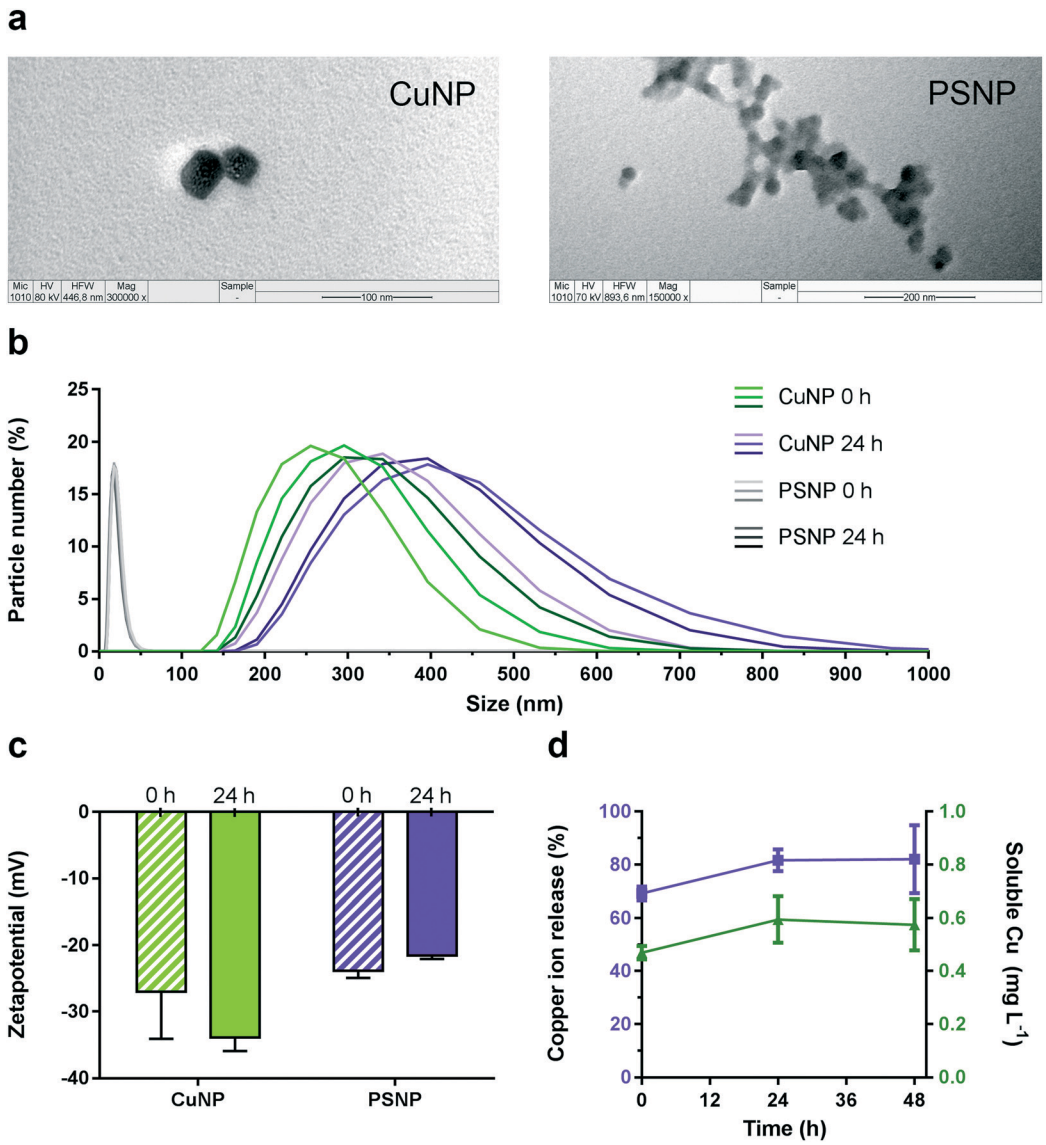

Fig. 1 Characterisation of CuNP and PSNP in exposure medium. (a) TEM image of 25 nm CuNP in egg water supplemented with SRHA (scale bar: 100 nm) and of 25 nm PSNP in egg water (scale bar: 200 nm) after 1 h of incubation. NP agglomerates in TEM images are not representative of what was found in the majority of the pictures but represents the picture with the best contrast to derive shape and size. (b) DLS profile showing the distribution of the hydrodynamic diameter of CuNP in egg water supplemented with SRHA and PSNP in egg water after 0 h and 24 h. (c) Zeta potential of CuNP and PSNP after 0 h and 24 h. (d) Dissolution profile of Cu over time of 1 mg L^{-1} CuNP in egg water supplemented with SRHA at different time points in % and mg L^{-1}. Error bars are + standard deviation (SD) of measured values for each exposure group consisting of 3 replicates.

Minteq (Table S2, ESI†). The addition of 30 mg L^{-1} SRHA to egg water resulted in a mean concentration of 12.9 ± 0.4 mg L^{-1} TOC (Fig. S2, ESI†). Deviations between measured concentrations and nominal concentration can be attributed to the filtration step while preparing the SRHA stock solution. Although the addition of SRHA to the CuNP suspension did not prevent clustering of particles, the distribution of the hydrodynamic diameters was smaller and more uniform than without addition of SRHA (Fig. 1b, Fig. S1a, ESI†). Moreover, the zeta potential remained more stable over time with SRHA, whereas it was closer to zero after 24 h in egg water only (Fig. S1b, ESI†). Taken together it can be concluded that the physicochemical characteristics of CuNP are altered towards a more stable colloidal suspension and free Cu^{2+} were significantly reduced upon addition of SRHA.

The total amount of copper measured in the exposure medium after 24 h was 0.08 ± 0.02 mg L^{-1} for 0.1 mg L^{-1} nominal CuNP (Fig. S1c, ESI†) and 0.73 ± 0.11 mg L^{-1} for 1 mg L^{-1} nominal CuNP (Fig. S1d, ESI†). Dissolution of free copper species after 24 h from 0.1 mg L^{-1} CuNP was 0.06 ± 0.01 mg L^{-1} and for 1 mg L^{-1} CuNP it was 0.59 ± 0.09 mg L^{-1}. The release of free copper species slightly increased over the first 24 h and remained stable afterward (Fig. 1d, ESI†). The concentration of $Cu(NO_3)_2$ was corresponding to the soluble copper

fraction in the CuNP solution as shown in Fig. S1d in the ESI.†

Uptake and effects during embryo development

During the first 72 h, zebrafish embryos develop within a chorion. Embryos exposed to CuNP and corresponding $Cu(NO_3)_2$ from 0–72 hpf showed the highest copper concentration in the chorion whereas in the embryo itself no increased copper concentration was measured in comparison to the control (Fig. 2a). This indicates the chorions protective role in the first 72 h and thus in subsequent experiments embryos were exposed after hatching. Remarkably, copper concentrations in chorions of CuNP exposed embryos were significantly higher than in $Cu(NO_3)_2$ exposed embryos, suggesting an increased accumulation of CuNP on the chorion (Fig. 2a). Likewise, after hatching (at 120 hpf) CuNP exposed embryos contain more copper than $Cu(NO_3)_2$ exposed embryos (Fig. 2b). Both the intestine and the skin epithelium seem to be surface areas with increased NP accumulation as PSNP accumulate in the gastrointestinal tract as well as in the cavity of lateral line neuromasts and on the tail epithelium (Fig. 3). Methods to visualize sites of accumulation used for CuNP and PSNP were not interchangeable, however, it is likely that both CuNP and PSNP accumulate on the outer epidermis and in the gastrointestinal tract.

Both CuNP and $Cu(NO_3)_2$ had similar effects on measured morphological endpoints. Both delayed the hatching success to the same extent (Fig. 2c). At 120 hpf, all embryos of both exposure groups were hatched, nonetheless, an equally impaired growth in both exposure groups was measured (Fig. 2d). PSNP exposure had no effect on the measured endpoints of embryo development.

Inflammatory responses

The inflammatory responses of embryos were assessed after waterborne exposure and injection. Further, the transcriptional alterations of waterborne exposed embryos were assessed in whole embryos and in intestinal tissue.

After waterborne exposure, whole embryo mRNA of pro-inflammatory cytokines (*irg1l*, *il1β*, and *tnfα*) were significantly altered after exposure to 10 mg L^{-1} PSNP and the chemokine *ccl20a* after exposure to PSNP, 1 mg L^{-1} CuNP, and

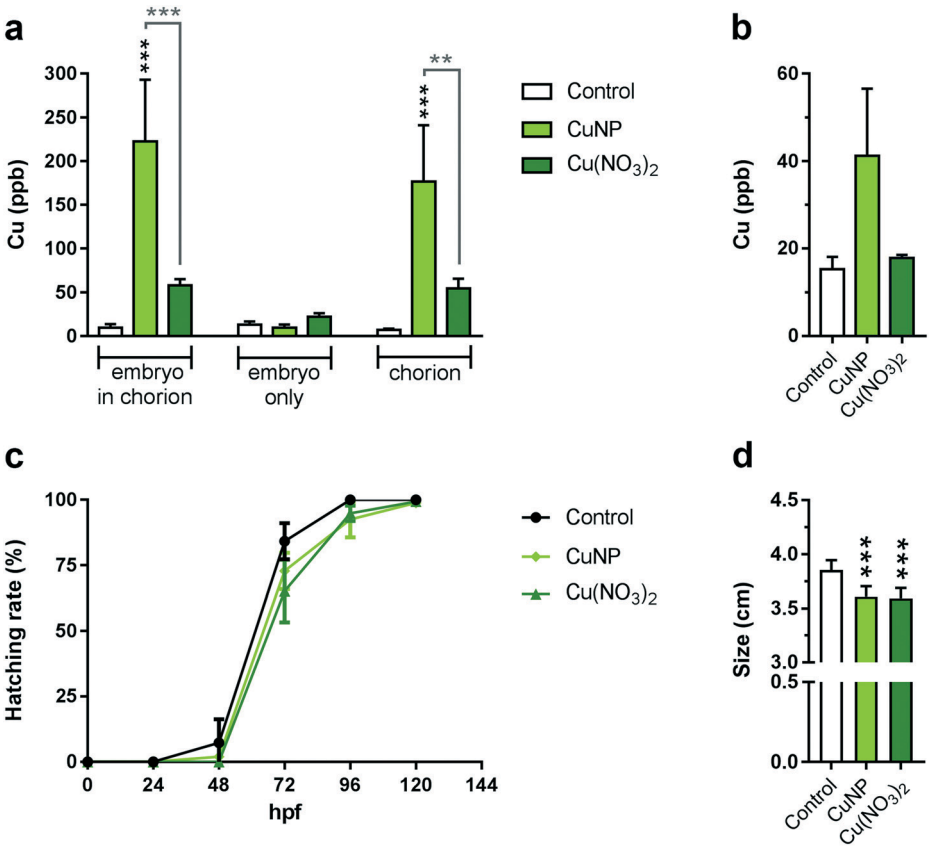

Fig. 2 Effects of CuNP and corresponding $Cu(NO_3)_2$ exposure on zebrafish embryo development. Zebrafish embryos were exposed to 1 mg L^{-1} CuNP and corresponding $Cu(NO_3)_2$ concentration (0.59 mg L^{-1}) form 0–120 hpf. (a) Total copper concentration in zebrafish embryos, dechorionated embryos, and chorions in μg per embryo at 72 hpf and (b) total copper concentration in zebrafish embryos at 120 hpf (n = 3). (c) Hatching rates of zebrafish embryos demonstrating equally delayed hatching success of zebrafish embryos exposed to CuNP and $Cu(NO_3)_2$ (n = 5, with 10 embryos per replicate). (d) Effect of 1 mg L^{-1} CuNP and corresponding $Cu(NO_3)_2$ on growth of zebrafish embryos measured as body length at 120 hpf (n = 10). Error bars are + standard deviation (SD) of measured values for each exposure group.

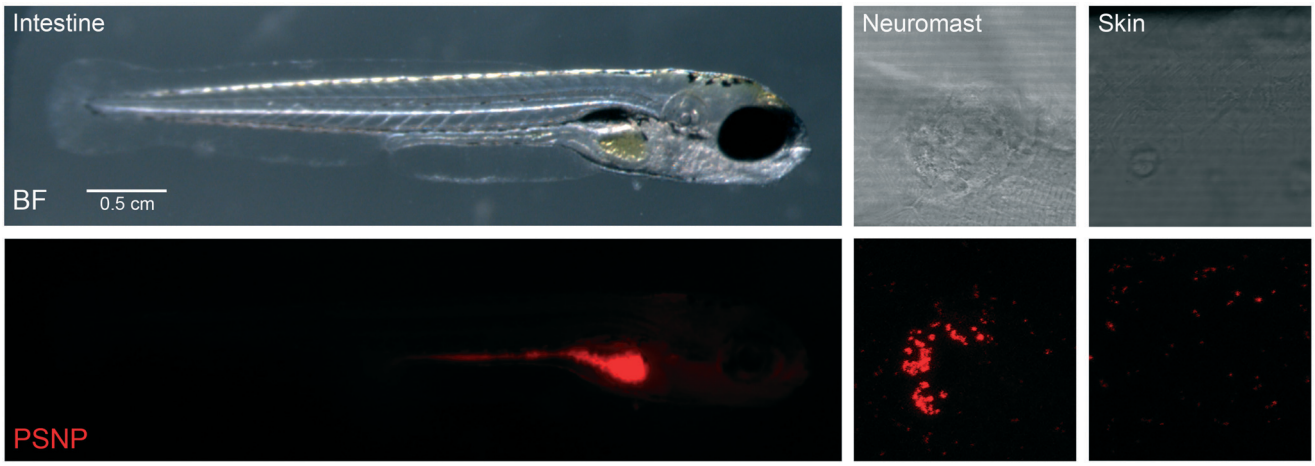

Fig. 3 Main target organs of PSNP accumulation in zebrafish embryo at 120 hpf. Representative fluorescence microscopy image depicting accumulation of PSNP (red) in the intestine and confocal microscopy images depicting PSNP accumulation in the cavity of a neuromast on the lateral line and skin (tail).

0.59 mg L^{-1} $Cu(NO_3)_2$ (Fig. S3a, ESI†). Contrariwise, only for CuNP, an increased number of neutrophils in the tail area was counted, although not significantly (Fig. S3b, ESI†). Whole body and tail imaging of fluorescently labeled neutrophils, macrophages, and *il1β* did not show any difference in comparison to control (Fig. S3c and d, ESI†).

When comparing intestinal tissue with body tissue (without intestine) of CuNP exposed embryos, a significant transcriptional upregulation of *il1β* and *irg1l* is measured for the body tissue (Fig. 4a), indicating stronger inflammatory responses in the body or skin cells. In accordance with that, confocal imaging of neuromasts on the skin cells revealed a higher expression of *il1β* in all exposures. Remarkably, the strongest signal of *il1β* was found in CuNP exposures, as depicted by increased intensity of the respective GFP tagged line (Fig. 4b). While the control, $Cu(NO_3)_2$, and PSNP exposed embryos have healthy skin cells composed by hexagonal cells, the structure is changed in the CuNP exposed embryos, indicating cell death and cell extrusion from the epithelium (Fig. 4b and S4a, ESI†). Imaging of the intestines showed that most of the *il1β* positive cells were macrophages surrounding the intestine in CuNP, as well to a minor extent in PSNP, exposed embryos. Close to a neuromast, a cluster of PSNPs was found to be engulfed by an activated macrophage, as it shows *tnfα* expression (Fig. S4b, ESI†). Tissue-specific expression of *irg1l* in the intestinal and dermal epithelium is shown by whole-mount *in situ* hybridization (Fig. 4c). In some embryos, *irg1l* was strongly expressed in extruded cell clusters surrounding the yolk and similar expressional patterns were found for *il1β* (Fig. S5a and b, ESI†) Transcriptional regulation of other genes, assessed by qPCR, is shown in Fig. S6 in the ESI.†

After injection of 1 nl of 0.5 mg L^{-1} CuNP and 1 mg L^{-1} PSNP, transcripts such as *il1β*, *soc3a*, and *ccl20a* were upregulated (Fig. 5a). In accordance with this, a significantly increased neutrophil recruitment in the tail area occurred (Fig. 5b). PSNP injection did not increase neutrophil recruitment. Additional transcriptional changes after injection can be found in Fig. S7 in the ESI.†

Discussion

Nanoparticles in an aqueous medium can be taken up by fish in numerous ways and therefore it is expected that initial effects occur at different sites. Here, we assessed dermal and intestinal inflammatory responses to both an inert polystyrene NP (PSNP) and a metal NP (CuNP). Although our efforts to assess potential inflammatory responses were not exhaustive, NP-specific responses were observed providing preliminary indications that nanoparticles can induce transcriptional alteration of pro-inflammatory genes in the skin cells and the tentative gut mucosa, and thus has potential suitability for use in adverse outcome pathways (AOPs).

Nanoparticle contribution to toxicity

The reactivity and toxicity of nanoparticles are dependent on their size in the test medium. Particle size has an inverse effect on the dissolution of metal NPs[28] and the smaller the NP the higher the chance of uptake across the cell membrane.[29] As ions are commonly more toxic, it is the ratio between these processes that determine the overall effect. In this study, CuNP clustered to agglomerates in a wide size-range. The agglomeration process is likely to be a dynamic process with small particles ready to contribute to a high dissolution rate and interact with biological surfaces, while bigger agglomerates might conciliate this effect. Thus, while ionic copper is known for inducing hair cell damage and inflammation in neuromasts of zebrafish,[30] the NPs present in the medium might add to this effect. All the three exposures, inert PSNP which remained as single NPs in solution, metallic CuNP, and $Cu(NO_3)_2$ elicited responses in the endpoints measured here and therefore it is concluded that it is a contribution of both particle and ionic metals.

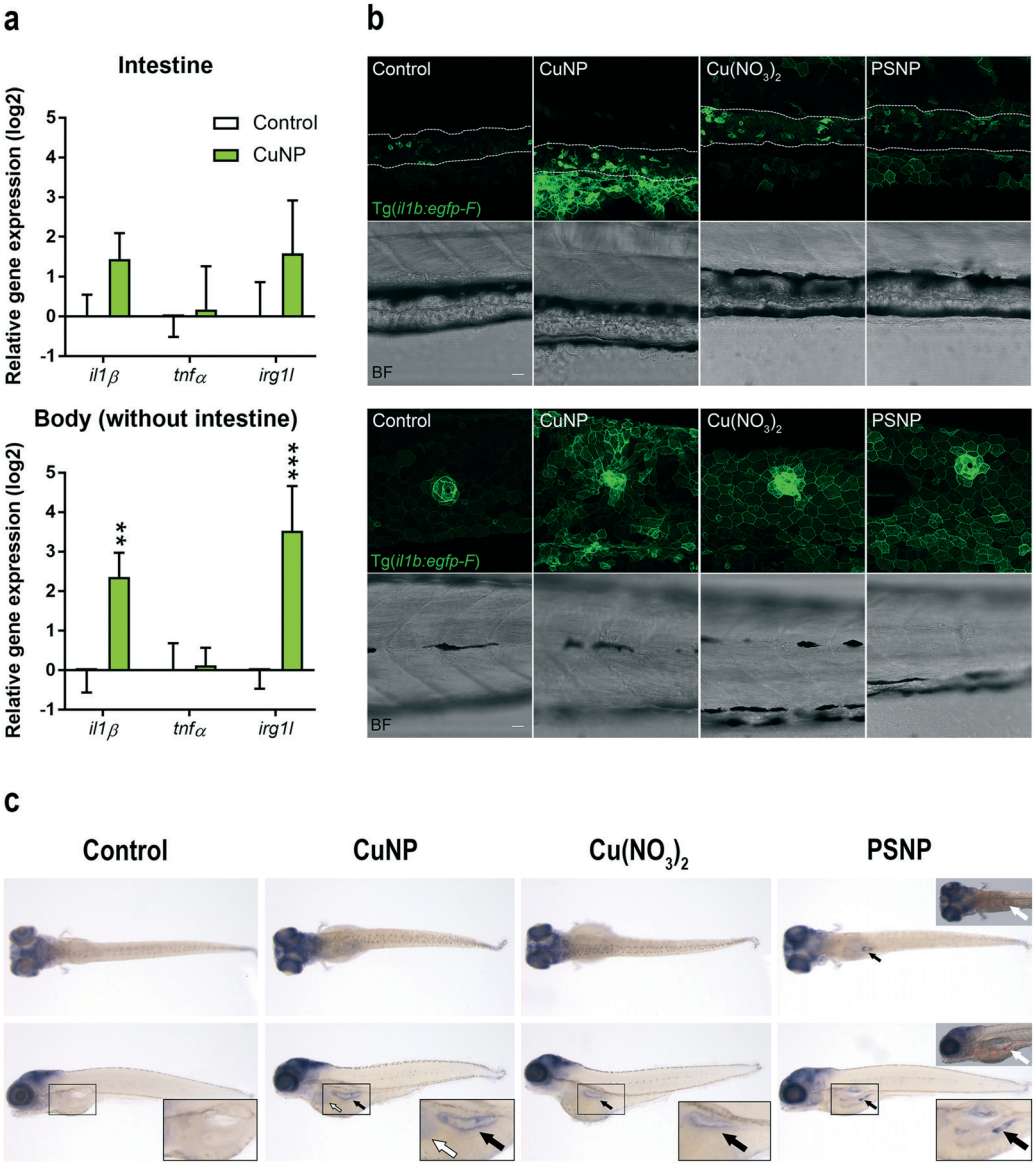

Fig. 4 Local expression of immune response regulated genes in embryonic intestine and skin after waterborne exposure from 72–120 hpf. (a) Transcriptional alterations of immune response related genes (*il1β*, *irg1l*, *tnfα*) in intestinal tissue and body tissue without intestine of wild-type zebrafish embryos exposed to 1 mg L^{-1} CuNP. Relative expression levels were normalized to *rpl13α*, calculated relative to expression levels in control embryos. Asterisks indicate significant differences to controls (*$p < 0.05$, **$p < 0.01$, and ***$p < 0.001$). Values are presented as mean ± SD (n = 3). (b) Representative images of caudal intestines (above) and neuromasts (below) of control with SRHA, 1 mg L^{-1} CuNP, corresponding $Cu(NO_3)_2$, and 10 mg L^{-1} PSNP waterborne exposed *Tg*(*il1b*:*eGFP-F*) embryos. Egg water control and SRHA control were similar. The transgenic reporter zebrafish line *Tg*(*il1b*:*eGFP-F*) expresses a membrane-targeted green fluorescent protein (GFP-F) under the control of the interleukin 1 beta (*il1β*) promoter. White lines delineate the intestine. CuNP exposed embryos display non-hexagonal shaped cells. Scale bars = 20 μm. (c) Representative images of *in situ* hybridization showing the expression profile of *irg1l* mRNA in wild-type zebrafish embryos after exposure to 1 mg L^{-1} CuNP, corresponding $Cu(NO_3)_2$ concentration, and 10 mg L^{-1} PSNP from 72–120 hpf. For PSNP exposure group a fluorescent microscope picture is inserted showing the presence of fluorescent particles (red; white arrow) in the intestine. Strongest staining was observed in the intestine after exposure to either CuNP, $Cu(NO_3)_2$, and PSNP (black arrow).

Innate immune responses in zebrafish skin

During the first three days of development, zebrafish embryos are protected by a chorionic layer that hampers nanoparticles and to a certain extent also metals from reaching the embryo.[31–33] In accordance with this, we found that a later stage of embryonic development is more suitable to assess mechanisms of action of nanoparticles as the chorion blocks particle and copper passage. After hatching, copper concentrations of CuNP exposed embryos were higher than in $Cu(NO_3)_2$ exposed embryos and PSNP accumulated on the skin, neuromasts, and in the intestine (Fig. 2b and 3), indicating an increased accumulation of CuNP and PSNP on outer or inner epithelial layers. The gills are not yet

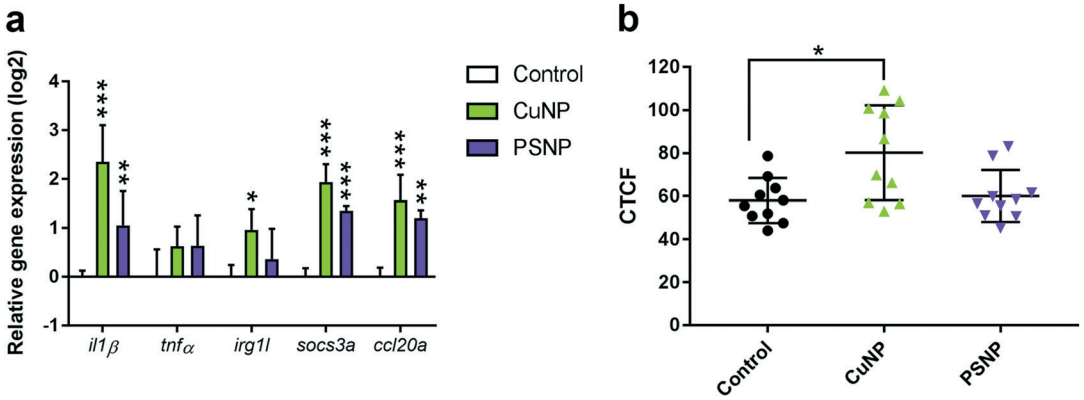

Fig. 5 Inflammatory responses in zebrafish embryos after injection of CuNP and PSNP. (a) Transcriptional alterations of immune response related genes (*il1β*, *tnfα*, *irg1l*, *socs3a*, *ccl20a*) in zebrafish embryos injected with 1 nl of 0.5 mg L^{-1} CuNP and 1 mg L^{-1} PSNP at 30 hpf and sampled 54 hpf. Relative expression levels were normalized to *rpl13α*, calculated relative to expression levels in control embryos. Values are presented as mean ± SD (n = 5). (b) Corrected total cell fluorescence (CTCF) of the tail area from *Tg*(*mpx*:*eGFP*) zebrafish embryos, in which GFP is expressed in neutrophils, injected with CuNP and PSNP at 30 hpf and imaged at 54 hpf. Values are presented as mean ± SD (n = 10). Asterisks indicate significant differences to controls (*$p < 0.05$, **$p < 0.01$, and ***$p < 0.001$).

functional and the skin cells are enriched with ionocytes (Na+–pump-rich cells) taking care of the osmoregulation and therefore transepithelial absorption of ions.[34] Although the skin primarily acts as a barrier, it is thus most likely, that the skin epithelium is one of the target organs for NPs or metals released from NPs.

With the adaptive immune system not yet being fully developed in zebrafish larvae,[35] the innate immunity is their first defense against invaders. Immune responses triggered by NPs is suggested to start with the recognition of the particle by Toll-like receptors[9] or fueled by the NPs generation of free radicals which both can initiate the secretion of cytokines such as *il1β* and *tnfα*. Our data show that *il1β*, was increasingly transcribed in skin cells and neuromasts of all exposed embryos, and in the body (without intestine) samples of CuNP exposed embryos, indicating the vulnerability of the outer epithelium. The expression of *il1β* around the neuromast was the most pronounced in CuNP and the membrane-bound *il1β* revealed damaged cellular structure resulting in cell death and cell extrusion from the epithelium (Fig. 4b) likely to cause function loss of the neuromasts as shown previously for metal NPs.[11] This was less pronounced in $Cu(NO_3)_2$ and PSNP treated embryos, leading to the conclusion that the response measured for CuNP is a combination of $Cu(NO_3)_2$ and NP activity. In accordance with this, the number of functional lateral line neuromasts is reduced to a higher extent in CuNP than in $CuSO_4$ exposed zebrafish embryos (96 hpf)[11] and mRNA levels of metallothionein and copper transporter are induced more in Cu_2O NP than in $CuCl_2$ treated zebrafish embryos (120 hpf).[36] It is remarkable that plastic NPs elicit an immune response on the epithelial membranes, which has not been reported so far. Furthermore, *il1β* is required for the recruitment of neutrophils,[23] which were increased in the tail area of at least the CuNP exposed larvae. The results found here are demonstrating consecutive events of a local innate immune responses for CuNP; from adsorption to outer epithelial layers and neuromasts to local induction of pro-inflammatory cytokines to the accumulation of neutrophils.

Innate immune responses in the intestine

A major target organ for NP accumulation is the intestine, as after hatching, larvae start to open their mouth and transition from yolk to external feeding. Accumulation of NPs in zebrafish larval intestines has been shown previously.[32] However, description of local mechanisms of actions is scarce. Özel *et al.* (2014)[37] report increased levels of intestinal serotonin secretion in zebrafish larvae after CuONP exposure, while TiO_2 and As-containing NPs increase intestinal ROS production in zebrafish larvae,[38,39] and AgNP can disrupt the epithelial mucosa and adversely affect the intestinal microbiota of adult zebrafish.[40] The latter may be related to immune responses as several studies indicate that induction of inflammation in zebrafish larvae intestines requires the presence of microbes.[41–43] To our knowledge, we provide the first evidence for gut-associated transcriptional changes of immune response-related genes after NP exposure in zebrafish embryos.

In the intestine of exposed zebrafish larvae, an increased local expression of *irg1l* for all exposure groups was found by *in situ* hybridization, which was also hinted by intestinal mRNA expression of CuNP exposed embryos. While a previous *in vitro* study provides evidence that soluble Cu is likely to be responsible for the induction of pro-inflammatory cytokines in intestinal cells,[44] there is no distinct difference between the intestinal *irg1l* expression of CuNP and $Cu(NO_3)_2$treatments in this study (Fig. 4c). Moreover, *irg1l* was altered to an even higher extent in body tissue without intestine samples (Fig. 4a), indicating the importance of the outer membrane. However, dermal expression of *irg1l* in *in situ* embryos was detected in only a few specimens which

might be reasoned with the loss of the loosely attached dermal cells (mucus; Fig. S5, ESI†) after the repeated washing steps or proteinase K digestion. Both the intestinal as well as the dermal cells are thus sites of action for NPs to induce immune responses. Overall, taking the expression of *il1β* in intestinal tissue (Fig. 4b) into account, responses appeared to be weaker in the intestine as compared to the skin cells or neuromasts.

Injection of NPs mimics the absorption into the organism which can occur at least for PSNP after waterborne exposure in juvenile zebrafish.[45] However, the internal concentration in fish in the environment remains speculative. While injection of both CuNP and PSNP in this study led to transcriptional alteration of several immune response-related genes, the number of neutrophils in the tail area was only increased in CuNP injected embryos. Previous studies indicated, however, that injected PSNPs can activate pathways related to immune responses when injected into the yolk of 2 days old zebrafish embryos (700 nm PSNPs) as well as in fathead minnow plasma (41 nm PSNP).[46,47] Because of the compliment activation by PSNP,[46] a much earlier response by macrophages could occur, which is not captured after 24 h of exposure in this study or alternatively plastic particles might be ingested by non-immune cells which was exemplified by Hosseini and colleagues.[48]

Innate immune responses in zebrafish as a key event in AOP

Here we show that different NPs elicit similar inflammatory responses in the tissues affected, particularly the intestine, the skin, and neuromasts. These observations may be of relevance to the efforts to develop compound agnostic AOPs, and our data provide potential starting points for such efforts by demonstrating the induction of recognized inflammatory markers. The next steps would be to develop quantifiable assays for the level of induction in order to formalize them as key events, which could be based on standardized microscopy or by transcriptional approaches. Further steps would involve ascertaining the adverse outcome at individual or population levels, as well as the determination of the molecular initiation event which sets off the inflammatory response.

In a developing fish, a contaminant-induced stress response will demand energy sources that are otherwise allocated to growth and maintaining overall health. Such adverse outcomes may be initiated by several events (*e.g.* oxidative stress or inflammation) and can be triggered by various contaminants. To explore the NP-specific effects on overall health and allocated energy sources, we compared morphological endpoints such as hatching and growth. No difference between CuNP and $Cu(NO_3)_2$ was found here, whereas previous results indicate stronger effects on hatching from CuNP than corresponding soluble copper.[33,49] However, in this study, the detailed confocal imaging of *il1β*, a key player in the inflammatory response, shows clear differences in the two treatments around the neuromasts. Neuromasts are essential to detect water movements and thus sense approaching prey, interact socially, or move with the current (rheotaxis). Several NPs, including TiO_2NP, AgNP, and CuNP as well as soluble copper has the potential to activate apoptotic cell death around lateral line neuromasts and ionocytes which was associated with a reduced ability to orientate in a current.[11–13,39] It is thus conceivable that NPs accumulating and affecting neuromasts induce behavioral changes as an adverse outcome, which has been reported previously for CuNP,[50] AgNP,[51] and PSNP[52] and was related to neurotoxicity. Our data add to evidence that PSNPs, and likely also CuNPs, accumulate in neuromasts where they are phagocytosed by macrophages (Fig. S4b, ESI†), resulting in local induction of pro-inflammatory cytokines, which may act as a precursor for damaged or apoptotic neuromasts leading to a potential adverse outcome. Focusing on inflammatory genes here, it is not excluded that oxidative stress plays a role too. A second adverse outcome related to NPs and immune responses may be immunosuppression, as shown by reduced host defense of adult fathead minnows exposed to TiO_2 NPs.[53]

Our data, therefore, suggest key biological target sites for NP exposed fish where an early key event, deregulation of innate immune responsive genes, potentially could lead to an adverse outcome such as a behavioral change. Furthermore, the screening of the neuromasts proved to be a suitable site to detect NP accumulation and inflammatory responses, and therefore it is suggested that screening of neuromast cells for acute inflammatory response in compound toxicity assessments can be extended to nanoparticles. The majority of particles showed adsorption to the outer membranes, specifically in the gut and skin cells and hence caused an acute inflammatory response. As a consequence, the Critical Body Residue approach,[54,55] allowing the relation to the internal accumulation of soluble chemicals to effects, is not applicable for these nanoparticle exposures. Taking the framework of building an Adverse Outcome Pathway[1] is a different approach that allows to mechanistically relate exposure to effects, and can potentially deal with low absorption potential in cells. Our study identifies target tissues of waterborne NP exposure and a set of key players of NP-related molecular effects, the immune marker genes *il1β*, *irg1l*, as well as neutrophil accumulation, suggesting possibilities to relate the induction of inflammatory responses to population-related endpoints. Yet the quantitative relationships on dose-responses relativeness of the key events should be determined as a next step. Also, lower concentrations might represent an environmental realistic scenario, although environmental concentrations of particularly nanoplastics are unknown so far.

Conclusions

Using a limited but representative set of inflammatory response markers, this study assessed dermal and intestinal inflammatory responses to both an inert polystyrene NP (PSNP) and a metal NP (CuNP). Obtained results provide the first evidence that nanoparticles can induce pro-inflammatory

responses in the skin and intestine cells. Responses were further observed to be more pronounced in the skin, indicating that the skin is more sensitive to NPs than previously anticipated. It can therefore, be speculated that inherent NPs-induced damage to neuromasts embedded in the lateral line can subsequently translate to behavioral changes, and thereby an adverse outcome at the population level. Transcriptional alterations of immune system regulating genes were observed for PSNPs, CuNP, and Cu ions, in which CuNP elicited the strongest response, indicating that both the nanoparticulate form and the metal ion contributed to the observed response. The potential of metal and plastic NP to induce innate immune responses in zebrafish embryos thus indicates that this mechanism of action, particularly in the skin, could prove suitable for screening purposes and serve as a building block in AOPs.

Conflicts of interest

There are no conflicts to declare.

Acknowledgements

We would like to thank Redmar Vlieg (Leiden University) for conducting 2-photon microscopy, Roel Heutink (Leiden University) for assistance in NP characterization, Marinda van Pomeren (Leiden University) for assistance in fish experimental work, and Ellard R. Hunting (Leiden University) for constructive feedback when writing the manuscript. The staff of the ZF facility of the Cell observatory is thanked for providing the experimental work environment. This study was funded by the Marie Skłodowska-Curie Fellowship (H2020-MSCA-IF-2014-655424) granted to Mónica Varela and the NWO-VIDI 864.13.010 granted to Martina G. Vijver.

References

1 S. C. Karcher, B. J. Harper, S. L. Harper, C. O. Hendren, M. R. Wiesner and G. V. Lowry, Visualization tool for correlating nanomaterial properties and biological responses in zebrafish, *Environ. Sci.: Nano*, 2016, **3**, 1280–1292.

2 G. T. Ankley, R. S. Bennett, R. J. Erickson, D. J. Hoff, M. W. Hornung, R. D. Johnson, D. R. Mount, J. W. Nichols, C. L. Russom and P. K. Schmieder, *et al.* Adverse outcome pathways: a conceptual framework to support ecotoxicology research and risk assessment, *Environ. Toxicol. Chem.*, 2010, **29**(3), 730–741.

3 S. Tedesco, H. Doyle, J. Blasco, G. Redmond and D. Sheehan, Oxidative stress and toxicity of gold nanoparticles in Mytilus edulis, *Aquat. Toxicol.*, 2010, **100**(2), 178–186.

4 S. George, S. Lin, Z. Ji, C. R. Thomas, L. Li, M. Mecklenburg, H. Meng, X. Wang, H. Zhang and T. Xia, *et al.* Surface defects on plate-shaped silver nanoparticles contribute to its hazard potential in a fish gill cell line and zebrafish embryos, *ACS Nano*, 2012, **6**(5), 3745–3759.

5 G. A. Dominguez, S. E. Lohse, M. D. Torelli, C. J. Murphy, R. J. Hamers, G. Orr and R. D. Klaper, Effects of charge and surface ligand properties of nanoparticles on oxidative stress and gene expression within the gut of Daphnia magna, *Aquat. Toxicol.*, 2015, **162**, 1–9.

6 R. van Aerle, A. Lange, A. Moorhouse, K. Paszkiewicz, K. Ball, B. D. Johnston, E. de-Bastos, T. Booth, C. R. Tyler and E. M. Santos, *et al.* Molecular mechanisms of toxicity of silver nanoparticles in zebrafish embryos, *Environ. Sci. Technol.*, 2013, **47**(14), 8005–8014.

7 N. R. N. R. Brun, M. Lenz, B. Wehrli and K. Fent, Comparative effects of zinc oxide nanoparticles and dissolved zinc on zebrafish embryos and eleuthero-embryos: Importance of zinc ions, *Sci. Total Environ.*, 2014, **476–477**, 657–666.

8 P. Khanna, C. Ong, B. Bay and G. Baeg, Nanotoxicity: An Interplay of Oxidative Stress, Inflammation and Cell Death, *Nanomaterials*, 2015, **5**(3), 1163–1180.

9 M. Turabekova, B. Rasulev, M. Theodore, J. Jackman, D. Leszczynska and J. Leszczynski, Immunotoxicity of nanoparticles: a computational study suggests that CNTs and C60 fullerenes might be recognized as pathogens by Toll-like receptors, *Nanoscale*, 2014, **6**, 3488–3495.

10 M. van Pomeren, N. R. Brun, W. J. G. M. Peijnenburg and M. G. Vijver, Exploring uptake and biodistribution of polystyrene (nano)particles in zebrafish embryos at different developmental stages, *Aquat. Toxicol.*, 2017, **190**(February), 40–45.

11 P. L. McNeil, D. Boyle, T. B. Henry, R. D. Handy and K. A. Sloman, Effects of metal nanoparticles on the lateral line system and behaviour in early life stages of zebrafish (Danio rerio), *Aquat. Toxicol.*, 2014, **152**, 318–323.

12 P. P. Hernández, V. Moreno, F. A. Olivari and M. L. Allende, Sub-lethal concentrations of waterborne copper are toxic to lateral line neuromasts in zebrafish (Danio rerio), *Hear. Res.*, 2006, **213**(1–2), 1–10.

13 O. J. Osborne, K. Mukaigasa, H. Nakajima, B. Stolpe, I. Romer, U. Philips, I. Lynch, S. Mourabit, S. Hirose and J. R. Lead, *et al.* Sensory systems and ionocytes are targets for silver nanoparticle effects in fish, *Nanotoxicology*, 2016, **10**(9), 1276–1286.

14 T. Wang, X. Long, Z. Liu, Y. Cheng and S. Yan, Effect of copper nanoparticles and copper sulphate on oxidation stress, cell apoptosis and immune responses in the intestines of juvenile Epinephelus coioides, *Fish Shellfish Immunol.*, 2015, **44**(2), 674–682.

15 L. Truong, S. C. Tilton, T. Zaikova, E. Richman, K. M. Waters, J. E. Hutchison and R. L. Tanguay, Surface functionalities of gold nanoparticles impact embryonic gene expression responses, *Nanotoxicology*, 2013, **7**(2), 192–201.

16 J. Duan, Y. Yu, Y. Li, Y. Li, H. Liu, L. Jing, M. Yang, J. Wang, C. Li and Z. Sun, Low-dose exposure of silica nanoparticles induces cardiac dysfunction via neutrophil-mediated inflammation and cardiac contraction in zebrafish embryos, *Nanotoxicology*, 2015, **10**(5), 575–585.

17 S. A. Renshaw and N. S. Trede, A model 450 million years in the making: zebrafish and vertebrate immunity, *Dis. Models & Mech.*, 2012, **5**(1), 38–47.

18 Z. Wang, J. T. K. K. Quik, L. Song, E.-J. J. Van Den Brandhof, M. Wouterse and W. J. G. M. G. M. Peijnenburg, Humic substances alleviate the aquatic toxicity of polyvinylpyrrolidone-coated silver nanoparticles to organisms of different trophic levels, *Environ. Toxicol. Chem.*, 2015, **34**(6), 1239–1245.

19 L. Song, M. Connolly, M. L. Fernández-Cruz, M. G. Vijver, M. Fernández, E. Conde, G. R. de Snoo, W. J. G. M. Peijnenburg and J. M. Navas, Species-specific toxicity of copper nanoparticles among mammalian and piscine cell lines, *Nanotoxicology*, 2014, **8**(4), 383–393.

20 J. P. Gustafsson, 13 September 2015. *Visual MINTEQ Version 3.1*, Stockholm, Sweden, https://vminteq.lwr.kth.se/, (Accessed 20 January 2017).

21 N. D. Lawson and B. M. Weinstein, In vivo imaging of embryonic vascular development using transgenic zebrafish, *Dev. Biol.*, 2002, **248**(2), 307–318.

22 F. Ellett, L. Pase, J. W. Hayman, A. Andrianopoulos and G. J. Lieschke, mpeg1 promoter transgenes direct macrophage-lineage expression in zebrafish, *Blood*, 2011, **117**(4), e49–e56.

23 M. Nguyen-Chi, Q. T. Phan, C. Gonzalez, J.-F. Dubremetz, J.-P. Levraud and G. Lutfalla, Transient infection of the zebrafish notochord with E. coli induces chronic inflammation, *Dis. Models & Mech.*, 2014, 7(7), 871–882.

24 M. Nguyen-Chi, B. Laplace-Builhe, J. Travnickova, P. Luz-Crawford, G. Tejedor, Q. T. Phan, I. Duroux-Richard, J. P. Levraud, K. Kissa and G. Lutfalla, *et al.* Identification of polarized macrophage subsets in zebrafish, *eLife*, 2015, **4**(JULY 2015), 1–14.

25 M. D. Abràmoff, P. J. Magalhães and S. J. Ram, Image Processing with ImageJ, *Biophotonics Intern.*, 2004, **11**(7), 36–42.

26 C. Thisse and B. Thisse, High-resolution in situ hybridization to whole-mount zebrafish embryos, *Nat. Protoc.*, 2008, **3**(1), 59–69.

27 B. E. V. Koch, J. Stougaard and H. P. Spaink, Spatial and temporal expression patterns of chitinase genes in developing zebrafish embryos, *Gene Expression Patterns*, 2014, **14**, 69–77.

28 Y. Zhai, E. R. Hunting, M. Wouterse, W. J. G. M. Peijnenburgh and M. G. Vijver, Importance of exposure dynamics of metal-based nano-ZnO, -Cu and -Pb governing the metabolic potential of soil bacterial communities, *Ecotoxicol. Environ. Saf.*, 2017, **145**, 349–358.

29 M. Zhu, G. Nie, H. Meng, T. Xia, A. Nel and Y. Zhao, Physicochemical properties determine nanomaterial cellular uptake, transport, and fate, *Acc. Chem. Res.*, 2013, **46**(3), 622–631.

30 C. A. d'Alençon, O. A. Peña, C. Wittmann, V. E. Gallardo, R. A. Jones, F. Loosli, U. Liebel, C. Grabher and M. L. Allende, A high-throughput chemically induced inflammation assay in zebrafish, *BMC Biol.*, 2010, **8**, 151.

31 K. Fent, C. J. Weisbrod, A. Wirth-Heller and U. Pieles, Assessment of uptake and toxicity of fluorescent silica nanoparticles in zebrafish (Danio rerio) early life stages, *Aquat. Toxicol.*, 2010, **100**(2), 218–228.

32 M. van Pomeren, N. R. Brun, W. J. G. M. Peijnenburg and M. G. Vijver, Exploring uptake and biodistribution of polystyrene (nano)particles in zebrafish embryos at different developmental stages, *Aquat. Toxicol.*, 2017, **190**, 40–45.

33 E. B. Muller, S. Lin and R. M. Nisbet, Quantitative Adverse Outcome Pathway Analysis of Hatching in Zebrafish with CuO Nanoparticles, *Environ. Sci. Technol.*, 2015, **49**, 11817–11824.

34 M. Jänicke, T. J. Carney and M. Hammerschmidt, Foxi3 transcription factors and Notch signaling control the formation of skin ionocytes from epidermal precursors of the zebrafish embryo, *Dev. Biol.*, 2007, **307**(2), 258–271.

35 N. S. Trede, D. M. Langenau, D. Traver, A. T. Look and L. I. Zon, The use of zebrafish to understand immunity, *Immunity*, 2004, **20**(4), 367–379.

36 D. Chen, D. Zhang, J. C. Yu and K. M. Chan, Effects of Cu_2O nanoparticle and $CuCl_2$ on zebrafish larvae and a liver cell-line, *Aquat. Toxicol.*, 2011, **105**(3–4), 344–354.

37 R. E. Özel, K. N. Wallace and S. Andreescu, Alterations of intestinal serotonin following nanoparticle exposure in embryonic zebrafish, *Environ. Sci.: Nano*, 2014, **2014**(1), 27–36.

38 O. J. Osborne, S. Lin, W. Jiang, J. Chow, C. H. Chang, Z. Ji, X. Yu, S. Lin, T. Xia and A. E. Nel, Differential effect of micron- versus nanoscale III–V particulates and ionic species on the zebrafish gut, *Environ. Sci.: Nano*, 2017, **4**(6), 1350–1364.

39 X. He, W. G. Aker and H.-M. Hwang, An in vivo study on the photo-enhanced toxicities of S-doped TiO_2 nanoparticles to zebrafish embryos (Danio rerio) in terms of malformation, mortality, rheotaxis dysfunction, and DNA damage, *Nanotoxicology*, 2014, **8**, 185–195.

40 D. L. Merrifield, B. J. Shaw, G. M. Harper, I. P. Saoud, S. J. Davies, R. D. Handy and T. B. Henry, Ingestion of metal-nanoparticle contaminated food disrupts endogenous microbiota in zebrafish (Danio rerio), *Environ. Pollut.*, 2013, **174**, 157–163.

41 Q. He, L. Wang, F. Wang and Q. Li, Role of Gut Microbiota in a Zebrafish Model with chemically induced enterocolitis involving toll-like receptor signaling pathways, *Zebrafish*, 2014, **11**(3), 255–264.

42 S. H. Oehlers, M. V. Flores, C. J. Hall, K. E. Crosier and P. S. Crosier, Retinoic acid suppresses intestinal mucus production and exacerbates experimental enterocolitis, *Dis. Models & Mech.*, 2012, **5**(4), 457–467.

43 S. Brugman, The zebrafish as a model to study intestinal inflammation, *Dev. Comp. Immunol.*, 2016, **64**, 82–92.

44 J.-P. Piret, S. Vankoningsloo, J. Mejia, F. Noël, E. Boilan, F. Lambinon, C. C. Zouboulis, B. Masereel, S. Lucas and C. Saout, *et al.* Differential toxicity of copper (II) oxide nanoparticles of similar hydrodynamic diameter on human differentiated intestinal Caco-2 cell monolayers is correlated in part to copper release and shape, *Nanotoxicology*, 2012, **6**(7), 789–803.

45 L. M. Skjolding, G. Ašmonaitė, R. I. Jølck, T. L. Andresen, H. Selck, A. Baun and J. Sturve, Assessment of the importance

of exposure route for uptake and internal localization of fluorescent nanoparticles in zebrafish (Danio rerio) using light sheet microscopy, *Nanotoxicology*, 2017, **11**(3), 351–359.

46 W. J. Veneman, H. P. Spaink, N. R. Brun, T. Bosker and M. G. Vijver, Pathway analysis of systemic transcriptome responses to injected polystyrene particles in zebrafish larvae, *Aquat. Toxicol.*, 2017, **190**(July), 112–120.

47 A. C. Greven, T. Merk, F. Karagöz, K. Mohr, M. Klapper, B. Jovanović and D. Palić, Polycarbonate and polystyrene nanoplastic particles act as stressors to the innate immune system of fathead minnow (Pimephales promelas), *Environ. Toxicol. Chem.*, 2016, **35**(12), 3093–3100.

48 R. Hosseini, G. E. M. Lamers, H. M. Soltani, A. H. Meijer, H. P. Spaink and M. J. M. Schaaf, Efferocytosis and extrusion of leukocytes determine the progression of early mycobacterial pathogenesis, *J. Cell Sci.*, 2016, **129**(18), 3385–3395.

49 J. Hua, M. G. Vijver, F. Ahmad, M. Richardson and W. J. G. M. Peijnenburg, Toxicity of different-sized copper nano- and submicron particles and their shed copper ions to zebrafish embryos, *Environ. Toxicol. Chem.*, 2014, **33**(8), 1774–1782.

50 Y. Sun, G. Zhang, Z. He, Y. Wang, J. Cui and Y. Li, Effects of copper oxide nanoparticles on developing zebrafish embryos and larvae, *Int. J. Nanomed.*, 2016, **11**, 905–918.

51 N. Garcia-Reyero, A. J. Kennedy, B. L. Escalon, T. Habib, J. G. Laird, A. Rawat, S. Wiseman, M. Hecker, N. Denslow and J. A. Steevens, *et al.* Differential effects and potential adverse outcomes of ionic silver and silver nanoparticles in vivo and in vitro, *Environ. Sci. Technol.*, 2014, **48**, 4546–4555.

52 Q. Chen, M. Gundlach, S. Yang, J. Jiang, M. Velki, D. Yin and H. Hollert, Quantitative investigation of the mechanisms of microplastics and nanoplastics toward zebrafish larvae locomotor activity, *Sci. Total Environ.*, 2017, **584–585**, 1022–1031.

53 B. Jovanović, E. M. Whitley, K. Kimura, A. Crumpton and D. Palić, Titanium dioxide nanoparticles enhance mortality of fish exposed to bacterial pathogens, *Environ. Pollut.*, 2015, **203**, 153–164.

54 M. G. Barron, M. J. Anderson, J. Lipton and D. G. Dixon, Evaluation of critical body residue QSARS for predicting organic chemical toxicity to aquatic organisms, *SAR QSAR Environ. Res.*, 1997, **6**(1–2), 47–62.

55 L. S. McCarty, J. A. Arnot and D. Mackay, Evaluation of critical body residue data for acute narcosis in aquatic organisms, *Environ. Toxicol. Chem.*, 2013, **32**(10), 2301–2314.